Acta Oceanol. Sin., 2025, Vol. 44, No. 2, P. 1–13
https://doi.org/10.1007/s13131-024-2448-y

Numerical simulation study on the properties and source tracing of swells in the Gulf of Guinea

Fumin Xu[1, 2], Hanzheng Ya[1, 2*], Donglin Zhu[1, 3]

[1] College of Harbour, Coastal and Offshore Engineering, Hohai University, Nanjing 210024, China
[2] Key Laboratory of Coastal Disaster and Protection of Ministry of Education, Hohai University, Nanjing 210024, China
[3] Guangxi Key Laboratory of Maine Environmental Science, Guangxi Academy of Marine Sciences, Nanning 530007, China

Received 30 October 2024; accepted 26 March 2025

Abstract
Swells are critical concerns regarding safety, marine transportation, and coastal engineering construction of coastal countries along the Gulf of Guinea and have been scientific problems due to the lack of systematic theoretical, numerical, and observational research. In this study, a double nesting numerical model was constructed and validated from the Atlantic Ocean to the Gulf of Guinea based on simulating waves nearshore (SWAN) to explore the swell characteristics and source tracing in the Gulf of Guinea in winter and summer seasons from 2020 to 2021. Simulation results reveal that swells are stronger and deflect more to the west in winter than summer, even though they dominate in both seasons in the Gulf of Guinea in the S-SW directional range. Simulated two-dimensional (2D) wave spectral patterns not only clarify wave composition, variation, and propagation properties from the central South Atlantic Ocean to the Gulf of Guinea, but also distinguish swell strength and directional range in winter and summer. The NW wind events induce swells which spread toward the SSE-ESE direction from the North Atlantic Ocean, big wind source generates sustained and stable S-SW swells from the South Atlantic Ocean, and corresponding swell-influenced areas are discussed. The strongest swell event in the Gulf of Guinea during the simulation was used as a case study to trace its source. A strong clockwise wind vortex within the Roaring Forties induced these large swells in the Gulf of Guinea approximately 5.5 days later, and swell propagation formed a regular isoline of peak period distribution from the South Atlantic Ocean to the Gulf of Guinea in the SSW-SW direction.

Key words swells, simulating waves nearshore, double nesting numerical model, Gulf of Guinea, Atlantic Ocean, 2D wave spectra

Citation Xu Fumin, Ya Hanzheng, Zhu Donglin. 2025. Numerical simulation study on the properties and source tracing of swells in the Gulf of Guinea. Acta Oceanologica Sinica, 44(2): 1–13, doi: 10.1007/s13131-024-2448-y

1 Introduction

The Gulf of Guinea is in the eastern part of the Atlantic Ocean, with an equatorial low-pressure zone in the north and a southeast trade wind zone in the south. Complex atmospheric-ocean dynamic conditions and the specific location of the Gulf of Guinea cause the coast to be frequently affected by Atlantic Ocean waves (Almar et al., 2015). Long-term exposure to waves also gradually degrades coastal function, and highly and extremely vulnerable areas account for approximately 26.98% and 11.66% of the total coastline in the Gulf of Guinea (Aman et al., 2019), respectively. With the rapid economic development of countries around the Gulf of Guinea, the coastal environmental and engineering problems caused by waves have become increasingly serious, and studying the wave characteristics from the Atlantic Ocean to the Gulf of Guinea has become essential to countries around the Gulf of Guinea.

Wave properties in the Gulf of Guinea are closely related to waves of the Atlantic Ocean, especially swells propagating from the Atlantic Ocean. Compared with wave studies in other regions, the lack of observations and the unique and complex wave composition and propagation hinder an in-depth understanding of waves from the Atlantic Ocean to the Gulf of Guinea. Gründlinch (1994)

Foundation item: The National Key R&D Program of China under contract No. 2023YFE0126300; the National Natural Science Foundation of China under contract Nos 42066002 and U20A2099.
*Corresponding author, E-mail: yahanzheng@126.com

analyzed the propagation and attenuation of waves in the South Atlantic based on satellite data, and the results show that the attenuation of waves and swells in the South Atlantic is approximately 1.2–3.9 m and 0.7–2.0 m per 1 000 km, respectively. Liu et al. (2002) carried out research on wind and wave characteristics in the South Atlantic based on data from 1950 to 1995 and analyzed wind, wave, and extreme wave frequencies in different seasons. Forristall et al. (2013) analyzed wind wave and swell components of spectral wave properties on the coast of West Africa in the West Africa Swell Project (WASP). Liu and Zhao (2019) found that swells in the South Atlantic are mostly concentrated in the eastern part near western African countries.

The wave system in the Gulf of Guinea is characterized by the coexistence of wind waves and swells at most of the time, with swells exerting dominant influence. Swells propagating from the Roaring Forties, a major swell system of the South Atlantic (approximately 40°S–60°S), are those which affect the wave system in the Gulf of Guinea, and the maximum swell wave height can reach approximately 3–4 m in the Gulf of Guinea (Prevosto et al., 2013). Swell systems in the Gulf of Guinea usually contained one or several swell components, such as swells generated in the Roaring Forties and the Southern Hemisphere trade wind zone (approximately 30°S–35°S) of the South Atlantic (Almar et al., 2015). The swell system in the coastal waters of the Gulf of Guinea is relatively stable, confirmed by wave research along the coast of Benin (Laïbi et al., 2014), a numerical simulation study of waves in most areas in the Gulf of Guinea by Wang and Zhang (2016) and statistical research of wave characteristics in the Niger Delta by Osinowo and Popoola (2021). All their achievements showed that the Gulf of Guinea was affected by fixed, medium-high energy SW swells year-round. Waves in the Gulf of Guinea are mainly propagated from the S-SW direction, and the northwest part of the Gulf of Guinea is seriously affected by swells originating in the high latitude of the South Atlantic (Zhou et al., 2021).

Even if some achievements of swell studies in the Gulf of Guinea have been conducted, some problems remain unsolved due to sparse observations and insufficient scientific research. (1) There are still insufficient numerical simulation studies on waves from the Atlantic Ocean to the Gulf of Guinea, especially the dynamic relationship of swells, i.e., swell wave propagation properties from the Atlantic Ocean to the Gulf of Guinea remain unclear. (2) Detailed wave spectral patterns and characteristics of the Atlantic Ocean swell impact on the Gulf of Guinea still need in-depth research. (3) The source tracing of swells in the Gulf of Guinea is still unclear since the present qualitative source tracing provides an obscure interpretation.

In this paper, Section 2 presents a double nesting simulating waves nearshore (SWAN) wave model system that has been established and validated. Section 3 presents the swell wave evolution and variations during propagation, including the proportion of the swell component in the Gulf of Guinea and the 2D wave spectral evolution during propagation from the Atlantic Ocean to the Gulf of Guinea in winter and summer seasons. Section 4 presents case studies to explore swell wave distributions and source tracing during propagation in both seasons. Section 5 provides the conclusions.

2 Model setup and validation

2.1 *Governing equation*

SWAN is a third-generation wave model developed by Delft University of Technology. The performance of SWAN has been continuously enhanced, and SWAN has become a numerical ocean wave model that is frequently used at various scales from the ocean scale to the coastal zone (Shi et al., 2021; Ye et al., 2022). The governing equation of SWAN can be expressed as

$$\frac{\partial}{\partial t}N+\frac{\partial}{\partial \lambda}C_{\lambda}N+(\cos\phi)^{-1}\frac{\partial}{\partial \phi}C_{\phi}\cos\phi N+\frac{\partial}{\partial \sigma}C_{\sigma}N+\frac{\partial}{\partial \theta}C_{\theta}N=\frac{S}{\sigma}, \quad (1)$$

where N is action density, which equals the energy density divided by the radian frequency ($N=E/\sigma$). E is energy density, σ is radian frequency. λ is longitude, ϕ is latitude, and θ is propagation direction, and t is time. The first term on the left side of this equation represents the local rate of change in the action density over time. The second and third terms represent the propagation of action density in geographical space (with propagation velocities C_{λ} and C_{ϕ} in the longitude and latitude directions, respectively). The fourth term represents the shifting of relative frequency due to variations in depths and currents (with propagation velocity C_{σ} in σ space), and the fifth term stands for the depth-induced and current-induced refraction (with propagation velocity C_{θ} in θ space). S is the total of source (sink) terms expressed as wave energy density, which includes the effects of generation, dissipation, and nonlinear wave-wave interactions.

2.2 *Nesting simulation domains and model setup*

A double nesting SWAN model was constructed to ensure that the wave energy input from the outside model of the Atlantic Ocean is not lost during simulation when the boundary conditions are set as zero. The outer domain (the Atlantic Ocean) and inner domain (domain of the Gulf of Guinea) are set as D1 (75°N–75°S, 83°W–22°E) and D2 (20°N–20°S, 20°W–15°E), respectively, as shown in Fig. 1.

The topography is obtained from ETOPO1 data, and the driven winds are provided by cross-calibrated multi-platform (CCMP) wind data. The spatial and temporal resolutions of CCMP winds are 0.25° × 0.25° and 6 h, re-

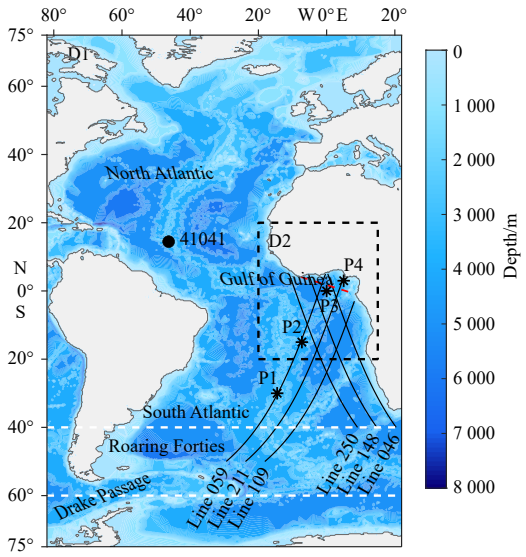

Fig. 1. Nesting model domains, observation buoy and satellite tracks of Jason-3. Symbol "•" is the wave buoy, the black solid lines represent the satellite trajectories, and symbol "*" represents the research points.

spectively. The spatial resolutions of the outer domain (D1) and inner domain (D2) are 0.25° × 0.25° and 0.1° × 0.1°, respectively. The corresponding time steps are 15 minutes and 5 minutes, respectively. The spectral frequency is discretized into 33 grades ranging from 0.04 Hz to 0.50 Hz, and the logarithmic distribution ($f_{i+1} = \gamma f_i$, f_{i+1} and f_i represent adjacent frequencies, γ is a constant (about 1.1, which is related with frequency resolution and can be calculated by model) is adopted between adjacent frequencies. The spectral directional resolution is 10°. The model physics applies the bottom friction of Hasselmann et al. (1973) with a coefficient of 0.038 and the depth-induced wave breaking method of Battjes and Janssen (1978) with a coefficient of 0.73. The wind energy input adopts the method of Cavaleri and Rizzoli (1981), and the whitecapping term uses the method of Komen et al. (1984). The triad and quadruplet nonlinear wave-wave interactions use the lumped triad approximation (LTA) method (Eldeberky, 1996) and the discrete interaction approximation (DIA) approximation (Hasselmann et al., 1985), respectively. In the previous studies of waves in the Gulf of Guinea (Xu et al., 2022), numerical experiments were carried out, revealing that a cutoff frequency (smaller than 0.1 Hz) could generate reasonable results for distinguishing swells from mixed seas from the Atlantic Ocean to the Gulf of Guinea. The definitions of significant swell wave height and swell direction (peak wave direction) are presented in the SWAN document (https://swanmodel.sourceforge.io/online_doc/swanuse/swanuse.html).

2.3 *Model validation*

For the Gulf of Guinea, June to September (winter) experiences the most active waves of the year; waves during December to March (summer) were slightly weaker than those in winter, and April to May and October to November are the times of wave transition from weak to strong and from strong to weak, respectively (Liu et al., 2002). In this study, simulations were conducted for both winter and summer seasons from December 2020 to March 2021 (summer) and June to September 2021 (winter) for model validation and wave property study. Considering the simulation time required for model stability and the duration for Atlantic Ocean swells propagating into the Gulf of Guinea, the spinning time for model simulations is set to 15 days.

2.3.1 *Outer model validation with buoy observations*

Available wave observation data are relatively scarce within and near the Gulf of Guinea in the South Atlantic Ocean. The wave buoy 41041 (Fig. 1) in the North Atlantic Ocean provided by the National Data Buoy Center (NDBC) is the nearest buoy to the Gulf of Guinea, for which data are available and can be used for outer model validation. Figures 2 and 3 show comparisons of the simulated significant wave height and mean wave period with buoy observations at 41041 during the simulation time. Table 1 shows the correlation coefficient (CC), root-mean-square error (RMSE), and ratio of error (ER) of significant wave height and mean wave period between the simulation and observation at buoy 41041.

Table 1 shows that the CC values of both significant wave height and mean wave period exceed 0.82 and 0.78; the corresponding RMSE values are less than 0.48 m and 0.99 s; and ER values in the measurements are below 9.4% and 11.8%, respectively, between the simulation and observation data during winter and summer seasons. Figures 2 and 3, and Table 1 demonstrate that simulations

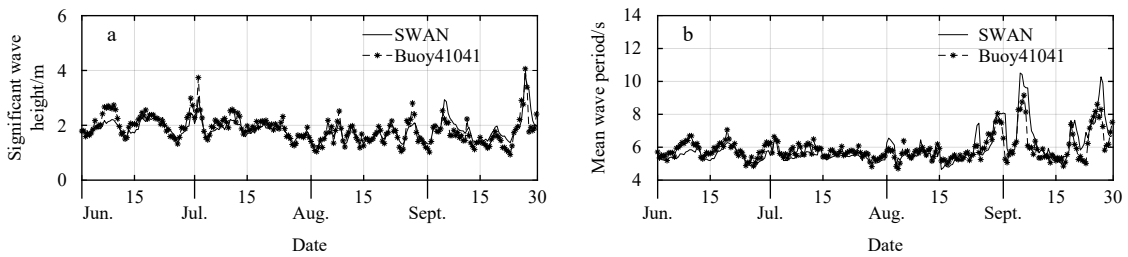

Fig. 2. Comparison of SWAN-simulated significant wave height (a) and mean wave period (b) with buoy 41041 in the winter season (June to September 2021).

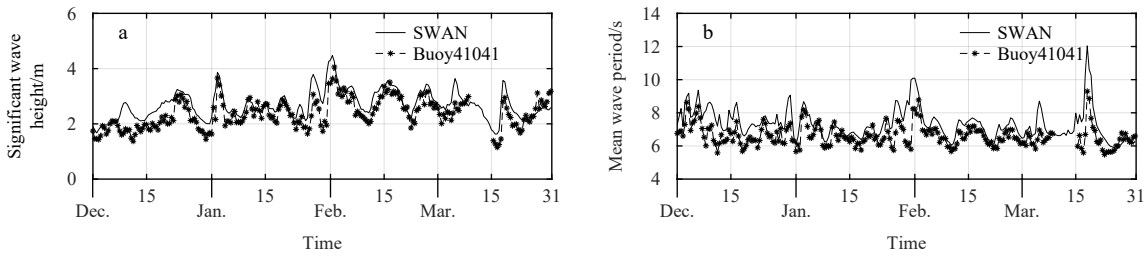

Fig. 3. Comparison of SWAN-simulated significant wave height (a) and mean wave period (b) with buoy 41041 in the summer season (December 2020 to March 2021).

Table 1. Error analysis of significant wave height and mean wave period between the simulation and observation at buoy 41041

Simulation season	CC_{H_s}	CC_{T_m}	$RMSE_{H_s}$/m	$RMSE_{T_m}$/s	ER_{H_s}/%	ER_{T_m}/%
Winter (Jun. to Sept. 2021)	0.88	0.81	0.27	0.67	7.7	8.5
Summer (Dec. 2020 to Mar. 2021)	0.82	0.78	0.48	0.99	9.4	11.8

Note: $ER_{H_s} = (H_{s_{sim}} - H_{s_{obs}}) / H_{s_{obs}}$; $ER_{T_m} = (T_{m_{sim}} - T_{m_{obs}}) / T_{m_{obs}}$. H_s and T_m are the significant wave height and mean wave period, and the subscripts of sim and obs represent the model simulation and the buoy observation, respectively.

during this summer season overestimate wave heights and wave periods compared to those in the winter season. Generally, the simulated significant wave height and mean wave period match the observations during both winter and summer simulations.

2.3.2 *Nesting model validation with satellite data*

Since the buoy validation mentioned above for the outer model is in the North Atlantic Ocean, which is far from the inner domain encompassing the Gulf of Guinea, Jason-3 satellite data were applied for supplementary validation of the nesting model validation from the South Atlantic Ocean to the Gulf of Guinea. Jason-3 is the fourth mission in the U.S.-European series of satellite missions that had measurements of the height of the ocean surface (https://sealevel.jpl.nasa.gov/missions/jason-3/).

According to the simulation results, the significant wave heights of the Gulf of Guinea are in the range of 1.48–3.24 m and 1.16–2.36 m in the winter and summer simulations, respectively. In this study, six satellite trajectories traversing from the South Atlantic Ocean to the Gulf of Guinea are selected, covering from the Roaring Forties to the Gulf of Guinea (Lines 059, 211, and 109) and the offshore of West Africa, where the South Atlantic swells are most concentrated (Lines 250,148, and 046) (as shown in Fig. 1). Two satellite cycles (from 1535 UTC on July 13, 2021, to 1333 UTC on July 23, 2021; from 1754 UTC on March 6, 2021 to 1553 UTC on March 16, 2021) covered the periods of the maximum wave strength in the Gulf of Guinea during winter (3.24 m at 0600 UTC on July 14, 2021) and summer (2.36 m at 0600 UTC on March 16, 2021), respectively; therefore, data of these six satellite lines are selected for validation of the nesting model.

Figures 4 and 5 show the comparisons of the simulated significant wave height and satellite data from the South Atlantic Ocean to the Gulf of Guinea in the winter and summer simulations within the cycle when the significant wave height in the Gulf of Guinea reaches the maximum values in both seasons. Tables 2 and 3 show the values of CC, RMSE, and ER between the simulated significant wave height and satellite data in winter and summer seasons.

The validations indicate that the simulated significant wave heights generally align with Jason-3 data, both in the South Atlantic Ocean and in the Gulf of Guinea, even though there are some deviations between the simulated results and the satellite. From Tables 2 and 3, it is evident that the simulated significant wave heights are generally consistent with satellite data. The average CC values between model simulation and satellite data exceed 0.92 and 0.86, the RMSE values are less than 0.39 m and 0.43 m, and the corresponding average ER values are about 9.7% and 14.5% in winter and summer seasons, respectively. Even though errors in individual satellite lines (for example, Line 059 as shown in Fig. 5b in summer) are relatively high, the simulation results generally align with satellite data along most of the satellite lines. The nesting model simulation is evidently reasonable both in the Atlantic Ocean domain and in the Gulf of Guinea domain. Therefore, this nesting model can be used for wave characteristics research from the South Atlantic Ocean to the Gulf of Guinea.

3 Swell wave evolution and variations during propagation from the Atlantic Ocean to the Gulf of Guinea

Dominant swells in the Gulf of Guinea usually originate from the Roaring Forties and the mid-latitude of the South Atlantic (Almar et al., 2015), in a S-SW direction (Prevosto et al., 2013; Laïbi et al., 2014). In this study, four research points (P1, P2, P3, and P4) were selected from the South Atlantic Ocean to the Gulf of Guinea (as shown in Fig. 1 and Table 4). Point P1 is located at 30°S

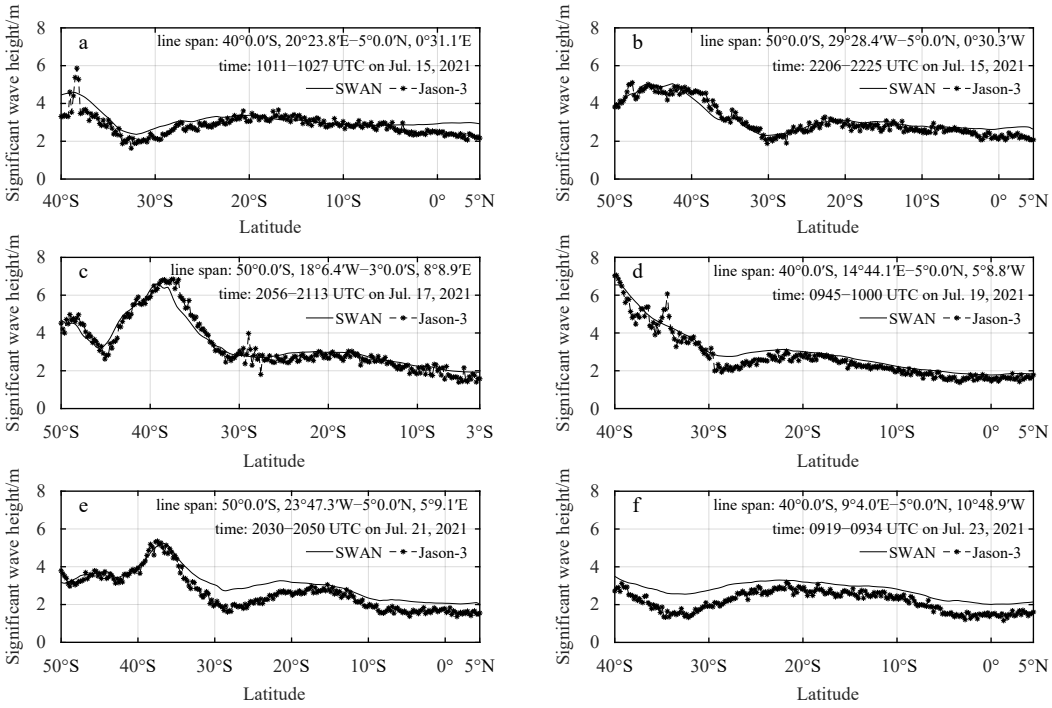

Fig. 4. Comparison of SWAN-simulated significant wave heights with Jason-3 data in winter, within the cycle when the maximum significant wave height in the Gulf of Guinea peaked (3.24 m), Line 046 (a), Line 059 (b), Line 109 (c), Line 148 (d), Line 211 (e) and Line 250 (f).

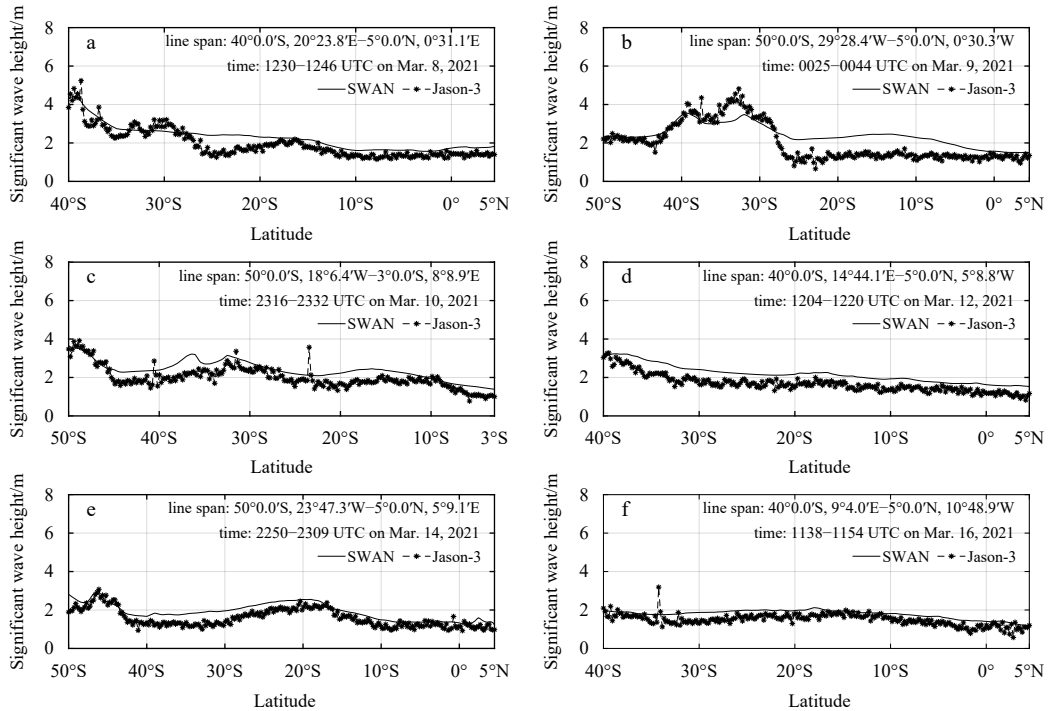

Fig. 5. Comparison of SWAN-simulated significant wave heights with Jason-3 data in summer, within the cycle when the maximum significant wave height in the Gulf of Guinea peaked (2.36 m), Line 046 (a), Line 059 (b), Line 109 (c), Line 148 (d), Line 211 (e) and Line 250 (f).

in the central part of the South Atlantic Ocean with strong swell components generated from the Roaring Forties and mid-latitude of the South Atlantic; Point P2 is located halfway between the Roaring Forties and the Gulf of Guinea to trace the route of swells towards the Gulf of Guinea; Point P3 and Point P4 are at the offshore and the nearshore of the Gulf of Guinea, which can be used to analyze the detailed wave characteristics when swells arrive at the offshore and the nearshore of the Gulf of Guinea. To investigate the swell propagation properties in detail,

Table 2. Error analysis of significant wave height between the model simulation and satellite observation data in winter season (June to September 2021)

Satellite line	Verification date	CC_{H_s}	$RMSE_{H_s}$/m	ER_{H_s}/%
Line 046	1011–1027 UTC on Jul. 15, 2021	0.77	0.39	9.1
Line 059	2206–2225 UTC on Jul. 15, 2021	0.95	0.31	7.0
Line 109	2056–2113 UTC on Jul. 17, 2021	0.97	0.38	7.8
Line 114	0945–1000 UTC on Jul. 19, 2021	0.97	0.40	9.9
Line 211	2030–2050 UTC on Jul. 21, 2021	0.95	0.40	10.1
Line 250	0919–0934 UTC on Jul. 23, 2021	0.90	0.47	14.5
	Average value	0.92	0.39	9.7

Note: $ER_{H_s} = (H_{s_{sim}} - H_{s_{obs}}) / H_{s_{obs}}$. H_s is the significant wave height, and the subscripts of sim and obs represent the model simulation and the buoy observation, respectively.

Table 3. Error analysis of significant wave height between the model simulation and satellite observation in summer season (December 2020 to March 2021)

Satellite line	Verification time	CC_{H_s}	$RMSE_{H_s}$/m	ER_{H_s}/%
Line 046	1230–1246 UTC on Mar. 8, 2021	0.90	0.40	12.6
Line 059	0025–0044 UTC on Mar. 9, 2021	0.85	0.67	20.4
Line 109	2316–2332 UTC on Mar. 10, 2021	0.87	0.42	13.4
Line 114	1204–1220 UTC on Mar. 12, 2021	0.92	0.41	13.9
Line 211	2250–2309 UTC on Mar. 14, 2021	0.88	0.33	13.3
Line 250	1138–1154 UTC on Mar. 16, 2021	0.74	0.32	13.4
	Average value	0.86	0.43	14.5

Note: $ER_{H_s} = (H_{s_{sim}} - H_{s_{obs}}) / H_{s_{obs}}$. H_s is the significant wave height, and the subscripts of sim and obs represent the model simulation and the buoy observation, respectively.

Table 4. Points selected from the South Atlantic Ocean to the Gulf of Guinea

Research points	Latitude	Longitude	Location
P1	30°00′S	14°30′W	30°S in the central of South Atlantic Ocean
P2	15°00′S	7°15′W	15°S in the central of South Atlantic Ocean
P3	0°00′	0°00′	Offshore the Gulf of Guinea
P4	3°00′N	5°00′E	Nearshore the Gulf of Guinea

all four points were generally arranged in a line around the S-SW direction from the South Atlantic Ocean to the Gulf of Guinea.

3.1 *Proportion of the swell component in the near shore Gulf of Guinea*

Figure 6 shows the proportions of significant swell wave height components and swell propagation directions in the inner Gulf of Guinea, as indicated within the red dashed lines of the Gulf of Guinea in Fig. 1, during the winter and summer simulations.

The ratio of the significant swell wave height to the total significant wave height (H_{swell}/H_s) ranges from 0.41 to 0.86 in the Gulf of Guinea in winter (Fig. 6a), and the corresponding H_{swell}/H_s ranges from 0.42 to 0.81 (Fig. 6b) in summer. At most of time, the ratio of the swell height to the total wave height is larger than 0.5 (the ratio is less than 0.5 occasionally). The long-period swells with large energy flux may induce disasters in coastal engineering even if the swell wave heights are not high enough. For example, the coastline from Côte d'Ivoire to Nigeria experiences a significant decline ranging from 2 m to more than 30 m per year under the influence of South Atlantic swells (Olugbenga et al., 2017). The ratios of the significant swell wave height to the total significant wave height in winter are higher than those in summer, with average values of 0.72 and 0.62, respectively. The swell propagation directions experience an increased fluctuation in winter than in summer. The swell propagation directions deviate slightly to the west in winter compared to summer, with average directions of 70.9 degrees and 68.8 degrees [in Cartesian convention, relative to the *x*-axis (toward the E direction) of the coordinate system (counterclockwise)] in winter and summer, respectively. Swells dominate almost constantly in the Gulf of Guinea, whether in winter or in summer; however, both the swell strengths and the swell propagation directions show slightly different behavior. The swell propagation directions during both seasons confirm that swells in the inner Gulf of Guinea must originate from sources in the South Atlantic Ocean.

3.2 *2D wave spectral evolution during propagation from the Atlantic Ocean to the Gulf of Guinea*

2D wave spectra at four points were simulated from the South Atlantic Ocean to the Gulf of Guinea in winter and summer to investigate wave composition, evolution, and distribution variations during propagation, especially

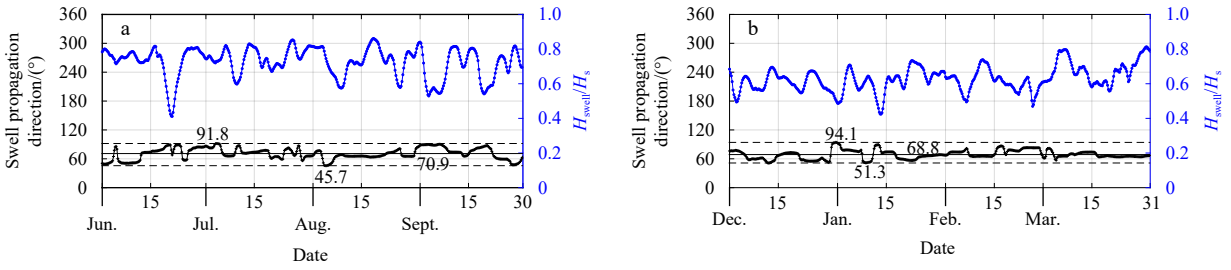

Fig. 6. Proportions of the swell component and swell propagation directions in the Gulf of Guinea during winter (a) and summer (b) simulations. H_{swell} is the significant swell wave height, and H_s is the total significant wave height.

focusing on the swell component. Spectral density was simulated at each spatial, frequency, and directional grid during winter and summer seasons. Consequently, the maximum spectral densities could be extracted at each frequency and direction grid point at each location, forming the swath map of the 2D spectral pattern in winter and summer seasons, as shown in Figs 7 and 8.

3.2.1 *2D wave spectral swath map in winter*

Figure 7 shows the 2D wave spectral swath map at points P1, P2, P3, and P4 in the winter simulation. Figure 7 illustrates that (1) the 2D spectra at point P1 show complicated wave compositions with wider band spectral wind waves and multiple-peak spectral swells. These wind waves and multiple-peak swells coexist, with wind waves distributed in all directions and swells covering most of the directions except the SW-S directional range. Wind waves are generated by the strong winds at this latitude, and swells originate from the South Atlantic Ocean far from the Roaring Forties. (2) At point P2, compared with point P1, both the spectral bands of wind waves and swells are significantly narrower with decreasing wind waves and swell strength. The swells are located within the NNW-ENE directional range with two strong swell events toward the N and NNE directions during the winter, and wind waves only distribute within the SW-ENE range. Evidently, there is a swell component propagating from the North Atlantic Ocean in a narrow SSE-SE directional range. (3) The 2D wave spectral swath maps at point P3 and point P4 show a single peak pattern of low-frequency swells toward the NW-ENE and NNW-ENE directions, respectively. These swell directions are relatively stable during winter, which means that waves mainly consist of a long period of swell waves from offshore to nearshore in the Gulf of Guinea during winter.

3.2.2 *2D wave spectral swath map in summer*

Figure 8 shows the 2D wave spectral swath maps at

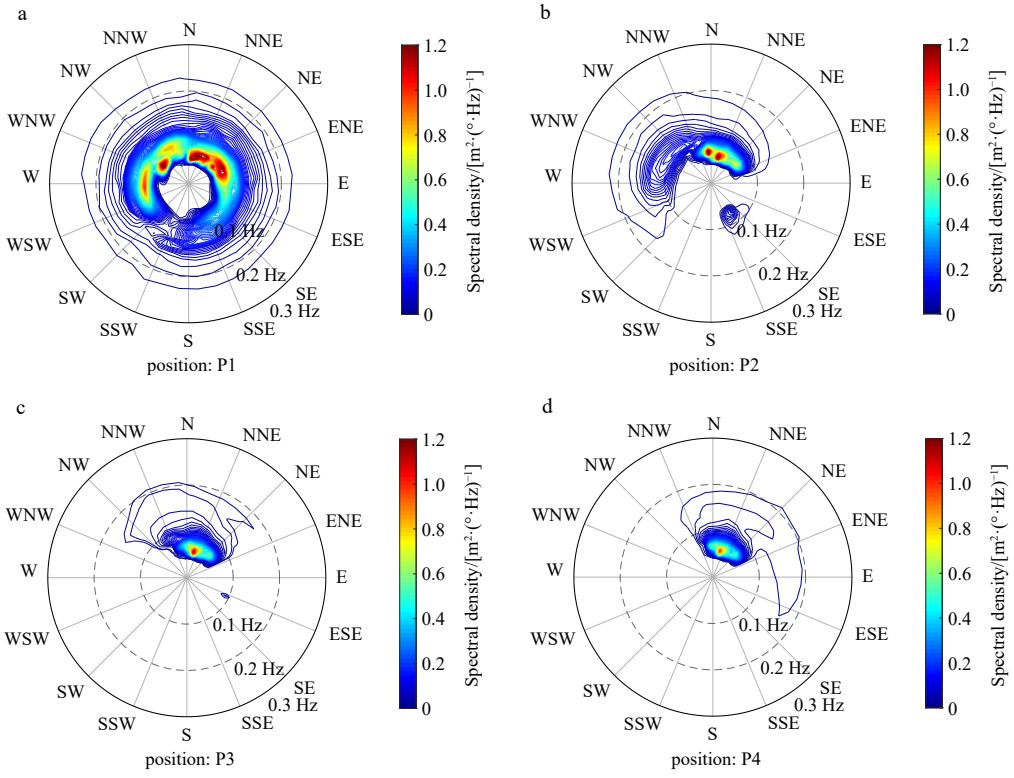

Fig. 7. Two-dimensional wave spectral swath map at points P1 (a), P2 (b), P3 (c), and P4 (d) in the winter simulation.

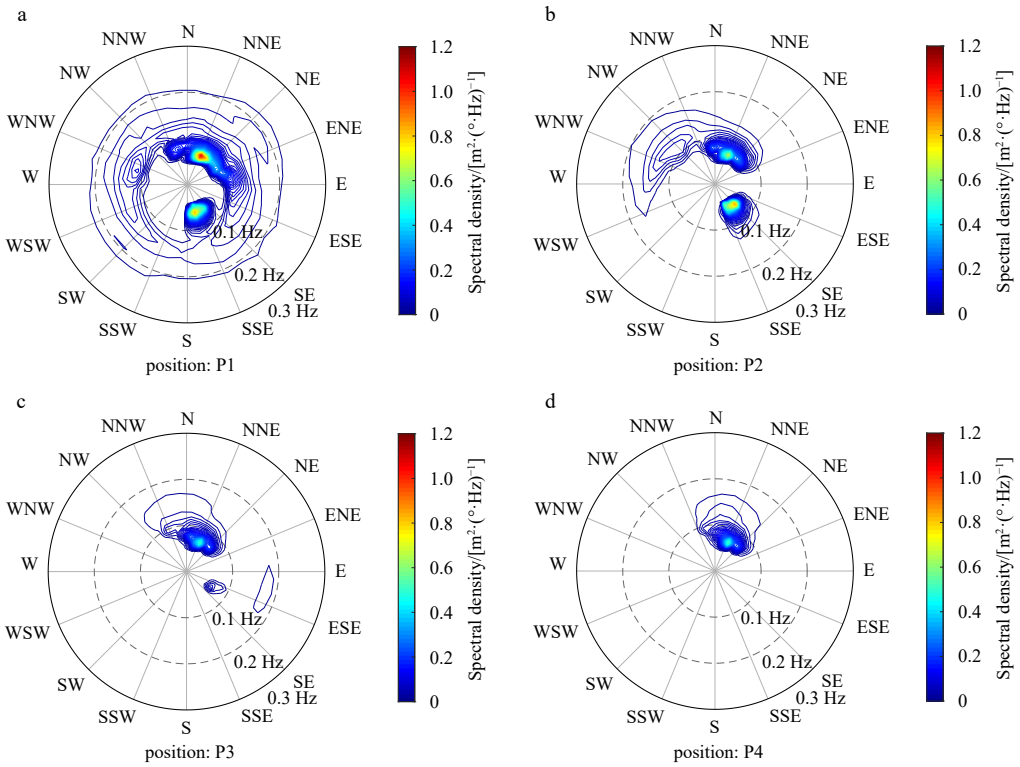

Fig. 8. Two-dimensional wave spectral swath map at points P1 (a), P2 (b), P3 (c) and P4 (d) in summer.

points P1, P2, P3, and P4 in summer. The results demonstrate that (1) the wind wave spectral component at point P1 covers all directions, approximately the same as that in winter. While the swell components mainly distribute within two directional ranges (ENE-NNW and S-SE), the two maximum spectral peaks imply that two large swell events occur during these directional ranges. ENE-NNW swells originate from the South Atlantic far from the Roaring Forties, and S-SE swells propagate from NW-N directions from the North Atlantic Ocean. (2) At point P2, the double peak swell swath patterns clearly have the same origins as those of P1. The strength of the S-SE swells is approximately the same as that of P1, while the strength of the ENE-NNW swells at P1 degenerates in both directional distribution and strength. Wind waves at P2 are confined within the WSW-ENE directions. The wave spectral evolutions at points P1 and P2 represent that the swells in the central South Atlantic Ocean during the summer season originate from two sources: one from the high latitudes of the South Atlantic Ocean far from the Roaring Forties (the swells to the ENE-NNW directions) and the other from the North Atlantic Ocean (the swells toward the S-SE directions). (3) The wave spectral swath patterns at points P3 and P4 show similar behavior with relatively high and narrow swell energy concentrating in the N-NE direction and a small proportion of wind wave components within the NNW-NE range. Compared with points P1 and P2, the S-SE directional swell spectral energy decreases dramatically to a small SE-ESE swell component offshore the Gulf of Guinea at point P3 and completely disappears at point P4. This means that the nearshore area of the Gulf of Guinea is not affected by the North Atlantic Ocean-generated swells.

3.2.3 *Comparison and analysis of the 2D wave spectral swath map in winter and summer*

From the above 2D wave spectral swath distributions in the central South Atlantic Ocean (points P1 and P2), offshore the Gulf of Guinea (point P3) and nearshore the Gulf of Guinea (point P4) in winter and summer seasons, the following are observed: (1) The wave compositions in the central South Atlantic Ocean are complicated during summer and winter seasons, and both wind waves and swells are relatively active. Wave complexity and strength become stronger when moving southward. Spectral wave swath density at the four points shows that swells in the nearshore area of the Gulf of Guinea propagate from the high latitude of the South Atlantic Ocean in winter and summer seasons without influence of swell components from the North Atlantic Ocean. In the offshore of the Gulf of Guinea, the North Atlantic Ocean swells show only a slight impact in the summer season in the simulation. (2) Swell systems are relatively narrow in the central South Atlantic Ocean in summer while swells propagate in a wider directional range in winter. (3) Swells in the central South Atlantic Ocean are stronger in winter than in summer, and North Atlantic Ocean-generated swells significantly impact the central South Atlantic Ocean in summer compared to winter. (4) The Gulf of Guinea is dominated by relatively stable swells which spread toward NNW-ENE direction in both winter and summer seasons, from offshore to nearshore zones, and these swells mainly prop-

agate from the high latitudes of the South Atlantic Ocean. Previous studies of wave characteristics in the Gulf of Guinea (Laïbi et al., 2014; Almar et al., 2015; Osinowo and Popoola, 2021) also indicated that the swell directions in the Gulf of Guinea were relatively stable and concentrated, both in the winter and summer.

The variation in swell strength and directions at the four points manifest that there always existed a stable swell system (toward the NNW-ENE direction) from the South Atlantic Ocean to the Gulf of Guinea. This means that swells offshore and nearshore of the Gulf of Guinea mainly source back to the same swells originating from the high latitude of the South Atlantic Ocean both in winter and summer. The reason is that high wind-generated waves frequently occur in the Roaring Forties and the mid-latitudes (approximately 20°S–40°S) of the South Atlantic Ocean due to the strong clockwise wind vortexes all year round, and part of these waves spread toward the NNW-ENE directions and finally propagate to the Gulf of Guinea.

4 Case study: swell wave distributions and source tracing during propagation

4.1 *Swells from the North Atlantic Ocean to the Gulf of Guinea*

As indicated by Figs 7 and 8, 2D wave spectral swath maps at points P2 and P3 show that swells in the South Atlantic and the Gulf of Guinea induced by the North Atlantic extreme weather events are not frequent cases. Two typical cases (when P2 experienced the maximum swells within the SSE-ESE scope during winter and summer simulation) are selected. The SSE-ESE directional swells shown in Figs 8 and 7 can be numerically located at 1200 UTC on February 7 and 0000 UTC on September 30, 2021, in the summer and winter, respectively, and the corresponding 2D spectra at points P2 and P3 are shown in Figs 9 and 10. From the wind fields of the Atlantic Ocean 10 days in advance of the two North Atlantic Ocean-induced swell events, the induced wind sources in the North Atlantic Ocean can be located for the two SSE-ESE directional swell systems at point P2.

Wind field distribution in the Atlantic Ocean shows that there are sustained strong NW high winds (>20 m/s) from January 29 to February 2 within the latitudes of 20°–60°N in advance of the SSE-ESE swell event at 1200 UTC February 7 and strong NW high winds (>20 m/s) from September 24 to September 25 within the latitudes of 40°–60°N in advance of the SSE–SE swell event at 0000 UTC September 30. Figure 11 presents the typical NW wind distributions in the Atlantic Ocean at 1200 UTC on February 2 and 0000 UTC on September 25. Clearly, these highly sustained NW winds generate large wind waves and then propagate in the NW direction as swells and finally enter the South Atlantic Ocean, inducing SSE-ESE directional swells in the central Atlantic Ocean at

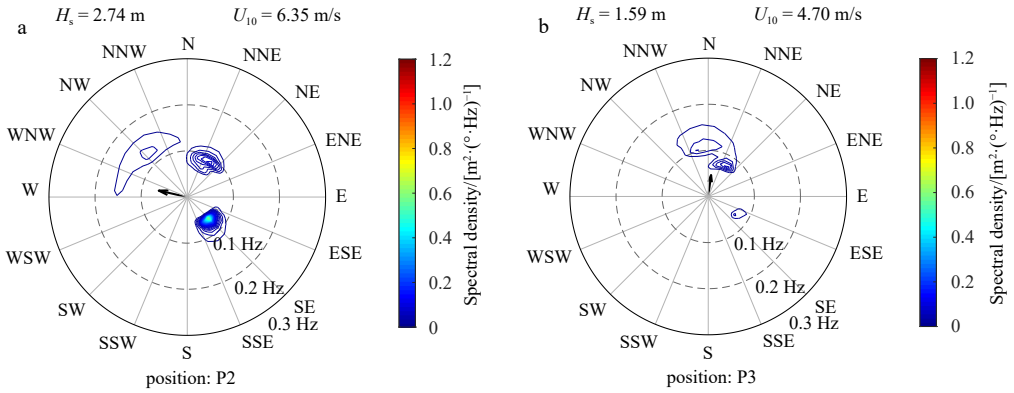

Fig. 9. Two-dimensional wave spectra at P2 (a) and P3 (b) at 1200 UTC on February 7 in summer.

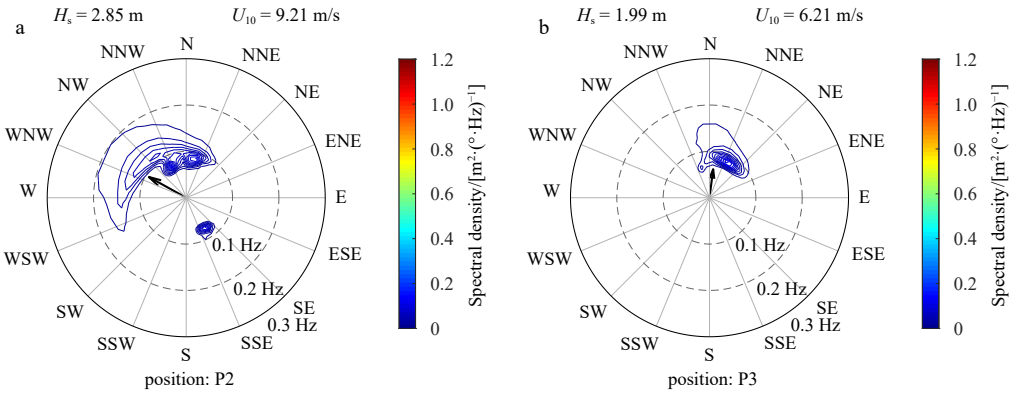

Fig. 10. Two-dimensional wave spectra at P2 (a) and P3 (b) at 0000 UTC September 30 in winter.

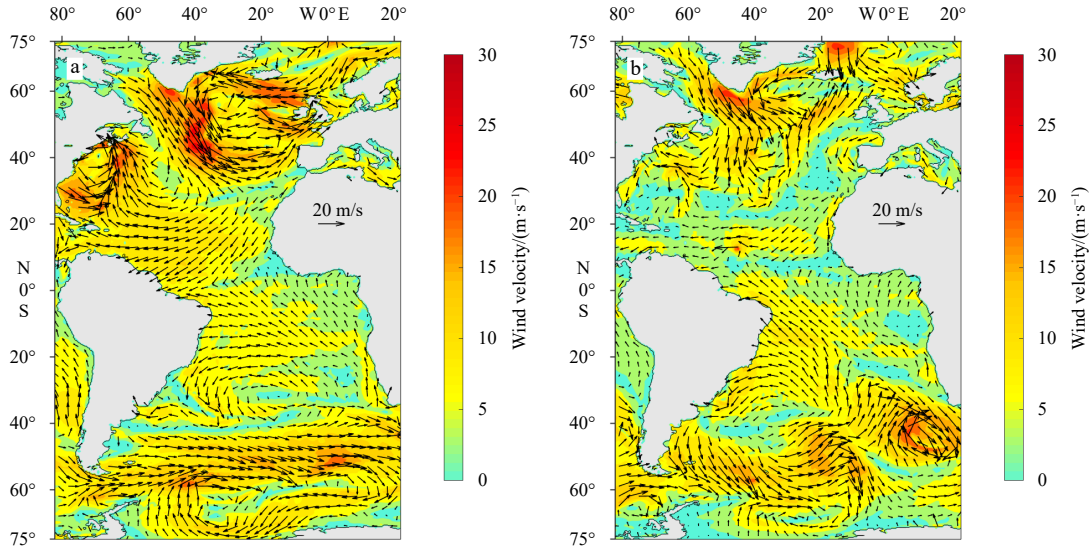

Fig. 11. Wind distribution in the Atlantic Ocean at 1200 UTC Feb 2 in summer (a) and 0000 UTC September 25 in winter (b).

point P2. Figures 7–10 show that the inner part of the Gulf of Guinea completely avoids these NW swells, with only slight swell energy offshore the Gulf of Guinea (point P3) from the North Atlantic Ocean, due to the sheltering effect by the west end of the Gulf of Guinea.

4.2 *Swells from the South Atlantic Ocean to the Gulf of Guinea*

To reveal the propagation property of swells from the South Atlantic Ocean to the Gulf of Guinea and trace the source of swells in the Gulf of Guinea, the maximum strength of swells in the Gulf of Guinea was selected (2.66 m, 0600 UTC on July 14 in winter) as typical case, and the genesis of swells in the South Atlantic Ocean and their trip northward to the Gulf of Guinea were investigated. Figure 12 presents the evolution of the wind field between the time of swell generation in the South Atlantic Ocean and the time of maximum swell wave height in the Gulf of Guinea. Figures 13 and 14 show the corresponding significant swell wave height and peak period, respectively.

At 1800 UTC on July 8, a strong clockwise wind vortex with a maximum wind velocity of more than 30 m/s occurred in the Roaring Forties (Fig. 12a), with a maximum significant swell wave height of approximately 8 m and a peak period of approximately 14 s (Figs 13a and 14a). The swells spread toward the N-NE direction, and different periods of swell components become separated. This strong clockwise wind vortex moved to the east and arrived at the eastern part of the South Atlantic Ocean until 1200 UTC on July 11, with significant swell wave heights of approximately 3–5 m and peak periods of approximately 14–16 s (Figs 13b and 14b). At 0600 UTC on July 14, the swell systems propagated to the Gulf of Guinea (Fig. 14c) and generated the strongest swell in the nearshore area of the Gulf of Guinea during the simulation time (Fig. 13c).

From the wind field from 1800 UTC on July 8 to 0600 UTC on July 14, it was found that there is no relationship between the swells and local wind waves in the Gulf of Guinea. Strong swells originated in the South Atlantic Ocean, particularly from the strong vortex winds in the

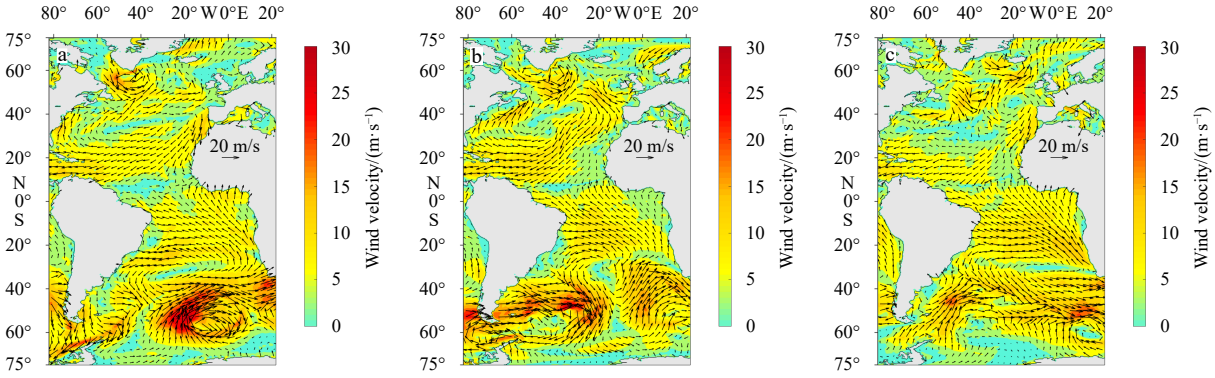

Fig. 12. Evolution of wind field between the time of swell generated in the South Atlantic Ocean and the time of maximum swell height in the Gulf of Guinea at 1800 UTC on July 8 (a), 1200 UTC on July 11 (b) and 0600 UTC on July 14 (c).

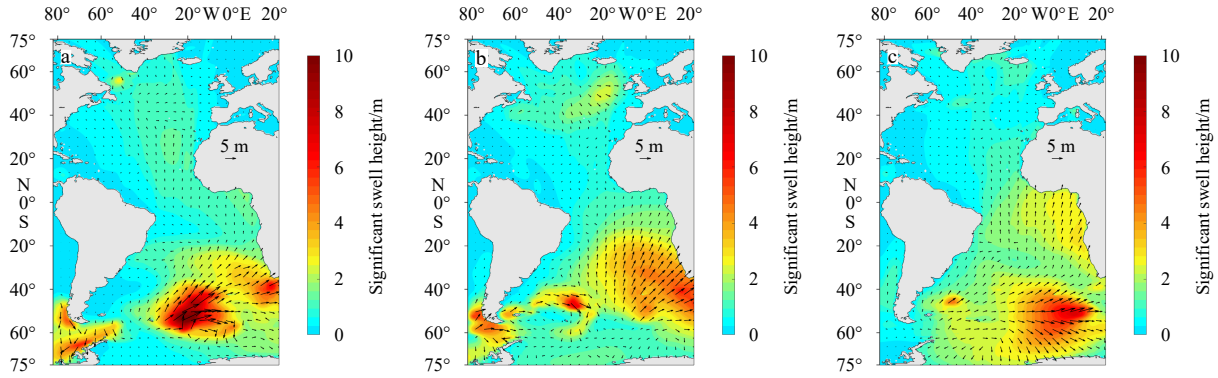

Fig. 13. Evolution of swell significant wave height between the time of swell generated in the South Atlantic Ocean and the time of maximum swell height in the Gulf of Guinea at 1800 UTC on July 8 (a), 1200 UTC on July 11 (b) and 0600 UTC on July 14 (c).

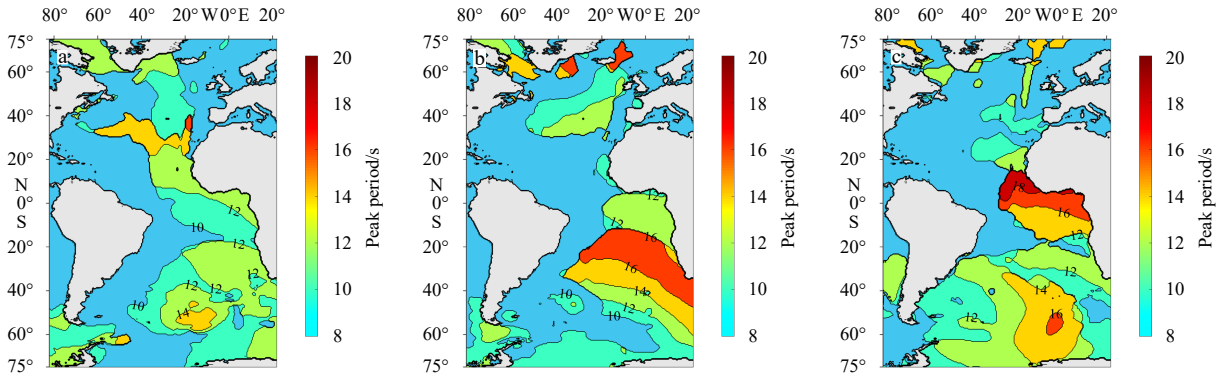

Fig. 14. Evolution of the peak period between the time of swell generation in the South Atlantic Ocean and the time of maximum swell height in the Gulf of Guinea at 1800 UTC on July 8 (a), 1200 UTC on July 11 (b) and 0600 UTC on July 14 (c).

Roaring Forties at 1800 UTC on July 8. The strongest swells in the Gulf of Guinea were propagated from the Roaring Forties of the South Atlantic Ocean approximately 5.5 days earlier (1800 UTC on July 8).

Figure 14 shows interesting swell distribution patterns when swells propagate from the South Atlantic Ocean to the Gulf of Guinea. The generated swell waves are in a regular distribution from the South Atlantic Ocean to the Gulf of Guinea in the SSW-SW direction, with the peak period increasing gradually on the way to the Gulf of Guinea. The reason is that swells with higher periods propagate faster than those with lower periods. Therefore, swells with longer periods enter the Gulf of Guinea earlier. The peak-period distribution demonstrates a clear illustration of the stratified swell distribution phenomena during propagation, clarifying the source of the swells in the Gulf of Guinea.

5 Conclusions

Waves from the Atlantic Ocean to the Gulf of Guinea in December 2020 to March 2021 (summer) and June 2021 to September 2021 (winter) were numerically simulated based on a double nesting SWAN model system, and the nesting model was validated by buoy observations and satellite data. A case study was carried out to investigate swell properties and source tracing during propagation from the North Atlantic Ocean and South Atlantic Ocean. Some new findings were obtained in this study: (1) swells in the Gulf of Guinea exhibit different behaviors in winter and summer seasons, even though swells dominate almost constantly in the Gulf of Guinea in winter and summer; (2) the 2D wave spectral evolution reveals clear swell and wind wave compositions and propagation patterns in both seasons during wave propagation from the Atlantic Ocean to the Gulf of Guinea; and (3) detailed 2D wave spectral analysis and wind source event tracing reveal that NW strong wind events from the North Atlantic can induce swells offshore in the Gulf of Guinea, both in winter and summer seasons. Major conclusions are as follows:

The Gulf of Guinea is dominated by S-SW swells propagating from the high latitudes of the South Atlantic Ocean in winter and summer seasons, while swell strengths are stronger in winter than in summer, with average ratios of swell significant height to total significant wave height of 0.72 and 0.62, respectively. The major swell directions in winter slightly deviate to the west by approximately 2.1 degrees on average.

Analysis of numerically simulated 2D spectra indi-

cates that swells in the central Atlantic Ocean can be influenced by swells within the SSE-ESE directional range, with only slight swell energy appearing offshore and no swells in the nearshore zone from the North Atlantic Ocean in winter and summer seasons. The protruding west shoreline of the Gulf of Guinea obstructs most of the North Atlantic Ocean swell propagating into the nearshore Gulf of Guinea. Stronger, longer sustained, and more southward NW winds in the North Atlantic Ocean can induce higher SSE-ESE swells in the central South Atlantic Ocean. North Atlantic Ocean wave-induced swells do not frequently occur compared to sustained and stable S-SW swells from the South Atlantic Ocean.

Stable and strong S-SW swells prevail from the South Atlantic Ocean to the Gulf of Guinea in winter and summer, and the simulated 2D spectra also exhibit that swells are significantly stronger in winter than in summer, originating from the central South Atlantic Ocean, extending offshore and nearshore to the Gulf of Guinea. In the simulation, the strongest swells were initially generated as large wind waves by the Roaring Forties wind (a large clockwise wind vortex) and then propagated toward the N-NE direction into the Gulf of Guinea.

Source tracing of the strongest swell in the Gulf of Guinea was studied. The combined analysis of the variation in significant wave swell height and peak period indicates that the source of the maximum swell system during the simulation time is originally induced by a strong clockwise vortex within the Roaring Forties in the South Atlantic approximately 5.5 days earlier. The swell peak period distributions form a regular isoline picture from the South Atlantic Ocean to the Gulf of Guinea in the SSW–SW direction, with peak period distributions increasing gradually towards the Gulf of Guinea. The propagation speeds of different swell periods facilitate these stratification phenomena, with longer periods of swells entering the Gulf of Guinea earlier.

Further research is still needed to explore the long-term wave trends from the Atlantic Ocean to the Gulf of Guinea, especially under the scenario of climate change. This study focuses on swell properties in the summer and winter seasons from 2020 to 2021; more seasonal simulations are needed to further illustrate seasonal scale swell behavior in the study area. The swell behavior during the conversion time also requires detailed research, and conducting seasonal wave simulations over multiple years can reveal additional general mechanisms of swells from the Atlantic Ocean to the Gulf of Guinea.

References

Almar R, Kestenare E, Reyns J, et al. 2015. Response of the Bight of Benin (Gulf of Guinea, West Africa) coastline to anthropogenic and natural forcing, part 1: wave climate variability and impacts on the longshore sediment transport. Continental Shelf Research, 110: 48–59, doi: 10.1016/j.csr.2015.09.020

Aman A, Tano R A, Toualy E, et al. 2019. Physical forcing induced coastal vulnerability along the Gulf of Guinea. Journal of Environmental Protection, 10(9): 1194–1211, doi: 10.4236/jep.2019.109071

Battjes J A, Janssen J. 1978. Energy loss and set-up due to breaking of random waves. In: Proceedings of 16th International Conference on Coastal Engineering. New York: American Society of Civil Engineers (ASCE), 569–587, doi: 10.1061/9780872621909.034

Cavaleri L, Rizzoli P M. 1981. Wind wave prediction in shallow water: theory and applications. Journal of Geophysical Research: Oceans, 86(C11): 10961–10973, doi: 10.1029/JC086iC11p10961

Eldeberky Y. 1996. Nonlinear transformation of wave spectra in the nearshore [dissertation]. Delft: Delft University of Technology

Forristall G Z, Ewans K, Olagnon M, et al. 2013. The West Africa Swell Project (WASP). In: Proceedings of the ASME 2013 32nd International Conference on Ocean, Offshore and Arctic Engineering. New York: American Society of Mechanical Engineers (ASME), doi: 10.1115/OMAE2013-11264

Gründlinch M L. 1994. Some characteristics of satellite-derived wave heights in the South Atlantic Ocean. Deep Sea Research Part I: Oceanographic Research Papers, 41(2): 413–428, doi: 10.1016/0967-0637(94)90011-6

Hasselmann K, Barnett T P, Bouws E, et al. 1973. Measurements of wind-wave growth and swell decay during the Joint North Sea wave Project (JONSWAP). Ergäenzungsheft zur Deutschen Hydrographischen Zeitschrift Reihe A 8(12). Hamburg: Deutsches Hydrographisches Institut, https://www.researchgate.net/publication/256197895

Hasselmann S, Hasselmann K, Allender J H, et al. 1985. Computations and Parameterizations of the Nonlinear Energy Transfer in a Gravity-Wave Specturm. Part Ⅱ: Parameterizations of the Nonlinear Energy Transfer for Application in Wave Models. Journal of Physical Oceanography, 15(11): 1378–1391, doi: 10.1175/1520-0485(1985)015<1378:CAPOTN>2.0.CO;2

Komen G J, Hasselmann S, Hasselmann K. 1984. On the existence of a fully developed wind-sea spectrum. Journal of Physical Oceanography, 14(8): 1271–1285, doi: 10.1175/1520-0485(1984)014<1271:OTEOAF>2.0.CO;2

Laïbi R A, Anthony E J, Almar R, et al. 2014. Longshore drift cell development on the human-impacted Bight of Benin sand barrier coast, West Africa. Journal of Coastal Research, 70(sp1): 78–83, doi: 10.2112/SI70-014.1

Liu Jinfang, Huang Hairen, Zhang Xiaohui, et al. 2002. An analysis of the annual variation of wind field and sea wave field in the South Atlantic Ocean. Transactions of Oceanology and Limnology (in Chinese), (3): 1–8

Liu Min, Zhao Dongliang. 2019. On the study of wave propagation and distribution in the global ocean. Journal of Ocean University of China, 18(4): 803–811, doi: 10.1007/

s11802-019-3827-4

Olugbenga A A, Gudmestad O T, Agbakwuru J. 2017. Swell description for Bonga offshore Nigeria location. Ocean Systems Engineering, 7(4): 345–369, doi: 10.12989/ose.2017.7.4.345

Osinowo A A, Popoola S O. 2021. Long-term spatio-temporal trends in extreme wave events in the Niger delta coastlines. Continental Shelf Research, 224: 104471, doi: 10.1016/j.csr.2021.104471

Prevosto M, Ewans K, Forristall G Z, et al. 2013. Swell genesis, modelling and measurements in West Africa. In: Proceedings of the ASME 2013 32nd International Conference on Ocean, Offshore and Arctic Engineering. New York: American Society of Mechanical Engineers (ASME), doi: 10.1115/OMAE2013-11201

Shi Qing, Tang Jun, Shen Yongming, et al. 2021. Numerical investigation of ocean waves generated by three typhoons in offshore China. Acta Oceanologica Sinica, 40(12): 125–134, doi: 10.1007/s13131-021-1868-1

Wang Kehua, Zhang Jun. 2016. Methods for determination of nearshore extreme wave for sea areas dominated by long period swells. China Harbour Engineering (in Chinese), 36(8): 11–15

Xu Fumin, Xing Tian, Zhou Xinwei, et al. 2022. Numerical simulation study on wave properties in the Gulf of Guinea. Journal of Waterway and Harbor (in Chinese), 43(5): 580–586, 595

Ye Qin, Yang Zhongliang, Bao Min. et al. 2022. Distribution characteristics of wave energy in the Zhe-Min coastal area. Acta Oceanologica Sinica, 41(5): 163–172, doi: 10.1007/s13131-021-1859-2

Zhou Xinwei, Xu Fumin, Zhang Jisheng. 2021. Wave property study in the Gulf of Guinea. China Harbour Engineering (in Chinese), 41(9): 1–6